Chemistry–A European Journal
Research Article
doi.org/10.1002/chem.202404630
Chemistry Europe
European Chemical Societies Publishing
www.chemeurj.org

Fragment-Based Approach for Hierarchical Nanotube Assembly of Small Molecules in Aqueous Phase

Ayisha Zia[+],[b] Meihui Yi[+],[a] Zhiyu Liu,[a] Fengbin Wang,*[b, c] and Bing Xu*[a]

A fragment-based approach has proven successful in drug design and protein assemblies, yet its potential for constructing biomaterials from simple organic building blocks remains underexplored, particularly for self-assembly in aqueous phases, where water disrupts intermolecular hydrogen bonding. To the best of our knowledge, this study introduces the first case of integrating fragments from self-assembling molecules to design a small organic molecule that forms novel hierarchical nanotubes with polymorphism. The molecule's compact design incorporates three structural motifs derived from known nanotube assemblies, enabling a hierarchical assembly process: individual molecules with two conformations form dimers, which organize into hexameric units. These hexamers further assemble into nanotubes comprising 2-, 5-, and 6-protofilament fibers. The nanofibers share a nearly identical asymmetric unit – a hexameric triangular plate – with similar axial and lateral interfaces. The lateral interface, involving interactions between phosphate groups and aromatic rings, exhibits plasticity, allowing slight rotational variations between adjacent units. This adaptability facilitates the formation of diverse nanofiber architectures, showcasing the flexibility of these systems in aqueous environments. By leveraging fragments of self-assembling molecules, this work demonstrates a straightforward strategy that combines conformational flexibility and self-assembling fragments to construct advanced supramolecular biomaterials from small organic building blocks in aqueous settings.

Introduction

This article reports the application of fragment-based approach for polymorphic hierarchical nanotubes of a small building block containing three distinct motifs and adopts two conformations. The development of supramolecular materials for biological applications has seen tremendous growth in recent years.[1] These advances have revealed that small organic molecules,[2] particularly short peptides,[3] are remarkably adept at self-assembling into higher-order structures in water. This property makes them valuable building blocks for the design of new biomaterials.[3–4] For example, building on the crystal structures of diphenylalanine (FF),[5] Gazit et al. showed that FF can self-assemble and form stiff nanotubes.[6] This seminal work inspired the development of short peptides as versatile building blocks for diverse supramolecular materials, leading to a vast array of self-assembled structures including ribbons,[7] tubes,[8] fibers,[9] and spheres.[10] Furthermore, recent advancements in cryo–EM structural determination have significantly enhanced our understanding of the nanotubes formed by these short peptides and their derivatives. Following the groundbreaking work of Conticello and Egelman, who utilized cryo–EM to reveal the structures of helical fibers comprised of coil-coil assemblies,[11] numerous cryo–EM structures of short peptides have been described.[12] For instance, cryo–EM helical reconstruction has been employed to elucidate the structure of filaments formed by a trimethylated heterochiral tetrapeptide containing diphenylalanine. These filaments exhibit distinct types of cross-β structures, with either C_7 or C_2 symmetry.[12a] More recently, the same technique has been applied to show that two dipeptides, one containing homochiral diphenylalanine and the other containing heterochiral diphenylalanine, form nanotubes with significantly different diameters – small and large, respectively.[12c]

While cryo–EM increasingly reveals atomic details of peptide nanotubes, a key question for rational design remains: how do small organic molecules assemble in water and what structures result? Can we use fragments from self-assembling small molecules to build new molecules that self-assemble in water, where water molecules severely interfere with intermolecular hydrogen bonding between the building blocks? The success of fragment-based drug design[13] and the seminal work on using this approach to build protein nanostructures[14] suggest that it is possible to apply fragment-based approach to create

[a] M. Yi,[+] Z. Liu, Prof. Dr. B. Xu
Department of Chemistry
Brandeis University
415 South Street, Waltham, MA 02453, USA
E-mail: bxu@brandeis.edu
[b] Dr. A. Zia,[+] Prof. Dr. F. Wang
Department of Biochemistry and Molecular Genetics
University of Alabama at Birmingham
Birmingham, AL, 35294, USA
E-mail: jerrywang@uab.edu
[c] Prof. Dr. F. Wang
O'Neal Comprehensive Cancer Center
University of Alabama at Birmingham
Birmingham, AL, 35294, USA
[+] Authors contributed equally.

Supporting information for this article is available on the WWW under https://doi.org/10.1002/chem.202404630

supramolecular nanostructures of small organic molecules in water. To test this idea, we combined three distinct fragments from known molecules that form nanotubes in water, intentionally avoiding diphenylalanine. This design yielded a small organic molecule, pBP–Bip–NBD (**1**, Scheme 1). Cryo–EM reveals that **1** adopts two distinct conformations. The two conformers first form dimers, which then organize into hexameric units. These hexamers further assemble into nanotubes that exhibit 2-, 5-, and 6-protofilament fibers. Despite this polymorphism, an almost identical building block (asymmetrical unit, ASU) is present in all three nanofibers, where six copies of molecule **1** form a triangle-shaped plate. The interactions between these plates are similar but have some flexibility, which enables the formation of the different nanotubes. Notably, **1** rapidly enters cancer cells and effectively inhibits immunosuppressive cancer cells.[15] This work illustrates an effective new way to design complex biomaterials by combining molecular flexibility with diverse self-assembling properties. The significance of using these fragments lies in their potential to harness pre-existing motifs known to self-assemble in water, which may enhance the ability to generate novel structures for biomaterials applications.

Results and Discussion

Many short peptide nanotubes have been reported on peptides containing the FF motif, where the phenylalanines contribute to π–π stacking in the nanotube architecture.[12] It is a reasonable hypothesis that aromatic compounds besides the FF motif or diphenylalanine could also promote self-assembly of peptide-like materials, as demonstrated in a few cases, including nanotubes formed by pBP–NBD,[16] amphiphilic cyanine dye,[17] and aromatic pyrene conjugated to sequences found in intrinsically disordered protein regions.[18] In the pBP–NBD structures, both biphenyl (BP) and NBD participate in π-stacking interactions along the filament. Such extensive π-stacking might be excessive to drive the self-assembly process. Indeed, it has been shown that both BP–ffsy and NBD–ffsy can self-assemble into nanofibers, with aromatic rings held together in the core by extensive π-stacking interactions.[12b]

Do all designed peptides always self-assemble into a homogenous, single type of nanofiber? The answer varies, and this variation can be directly observed using high-resolution cryo–EM. In the cases of pBP–NBD and BP–ffsy (Scheme 1), the self-assembled nanofibers are homogenous filaments under the reported conditions.[12b,16] In contrast, the product of NBD–ffsy exhibited polymorphic cross-β characteristics with four distinct species observed.[12b] We think this polymorphism depends on the aromatic core in two ways: (1) the number of local minima it can pack into as a filament core and (2) for a given packing core, the plasticity of the building block and whether it has multiple ways of further packing into nanofibers. To further investigate this and test the fragment-based approach, we selected pBP, BP, and NBD as three distinct fragments to construct a very compact self-assembling small molecule by connecting pBP and NBD to the N- and C-termini of biphenylalanine, respectively. This design resulted in molecule **1** (pBP–Bip–NBD).

Following established procedures,[15] we synthesized **1** and purified it with HPLC. To validate the self-assembly ability of molecule **1**, we employed negative staining transmission electron microscopy (TEM) to investigate fiber formation across various compound concentrations. The resulting images revealed fibers with diameters of approximately 5–8 nm at compound concentrations ranging from 50 to 200 μM in PBS buffer at pH 7.4. Aside from variations in fiber abundance, no apparent morphology differences were observed between the different concentrations (Figure 1). Although peptide concentration influences morphology to some extent, negative-stained TEM data cannot clearly distinguish 2-, 5-, or 6-protofilament structures. Cryo–EM analysis (Figure 2A) reveals that all three filament types coexist within the same sample, preventing a clear correlation between peptide concentration and filament abundance.

Recent advancements in cryo–EM have enabled researchers to not only determine the structures of peptide assemblies but also to distinguish between various morphologies for subsequent reconstruction.[19] Cryo–EM micrographs of self-assembled fibers from 20 μM molecule **1** reveal that these fibers are polymorphic, having multiple distinct classes (Figure 2A). Reference-free two-dimensional (2D) classifications further confirm this observation, showing three distinct classes (Figure 2B–D). The first class displays apparent cross-overs, a characteristic often observed in 2-protofilament amyloid fibers such as Aβ,[20] Tau,[21] and α-Synuclein.[22] The second and third classes both exhibit tubular features but differ in symmetry. The second class lacks a left-to-right mirror plane, suggesting its features originate from an odd Bessel order. In contrast, the third class possesses such a mirror plane, indicating features arising from an even Bessel order. For each class, potential helical symmetries were indexed from the averaged power spectrum of aligned raw particles. Through trial and error, each possible

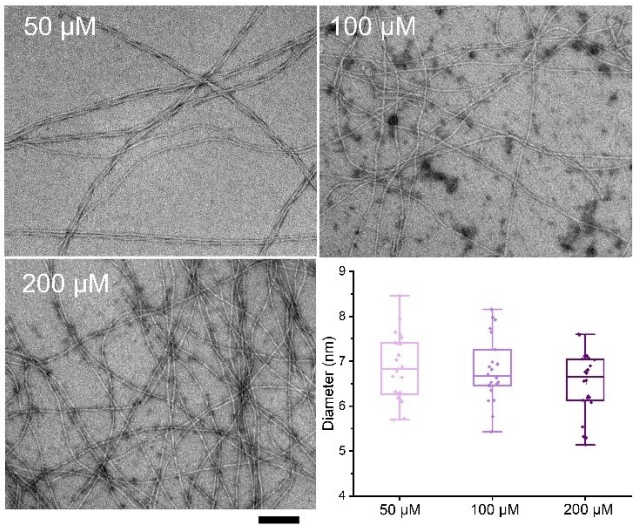

Figure 1. The TEM images of molecule **1** of different concentrations (50 μM, 100 μM, and 200 μM) in PBS buffer (pH 7.4) and the diameters analysis. The scale bar is 100 nm.

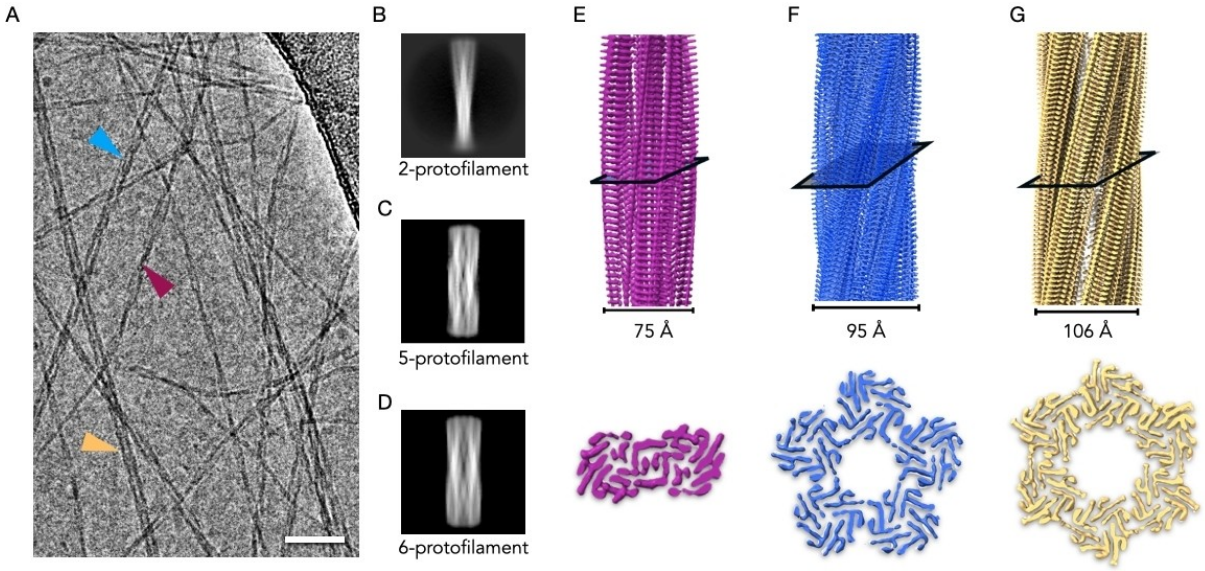

Figure 2. (A) Representative Cryo–EM micrograph displays the diversity of fiber arrangements, with different classes indicated by arrowheads. The scale bar is 50 nm. (B–D) Two-dimensional averages of three representative fiber classes, as highlighted in panel (A), are presented. (E–G) Three-dimensional helical reconstructions of these three classes at near-atomic resolution provide detailed structural information. The top panels show the filament view, while the bottom panels show the filament cross-section.

symmetry was tested, and the resulting volumes were visually examined for recognizable peptide-like features, such as backbone and side chain densities (Figure 2E–G). This analysis revealed that class 1 has C2 point group symmetry with a rise of 4.98 Å and a twist of 1.79°. Class 2 has C1 point group symmetry with a rise of 0.99 Å and a twist of 144.37°. Lastly, class 3 has C1 point group symmetry with a rise of 0.83 Å and a twist of −59.78°.

In single-particle cryo–EM, we collect 2D projections of 3D objects, resulting in the loss of handedness information. The correct handedness of the reconstructed volume is typically determined by observing the handedness of α-helices, if present, as all α-helices in proteins made of L-peptides are right-hand fibers. Therefore, we performed model building in volumes of both handedness and determined the correct handedness based on a higher real-space correlation coefficient (RSCC) and lower clash score. Helical reconstruction of these three volumes reached resolutions of 3.6 Å, 2.8 Å, and 2.8 Å, respectively, as judged by map:map FSC (Table S1, supplemental Figure 1). The 3D volumes clearly indicate that classes 1, 2, and 3 possess 2-protofilament, 5-protofilament, and 6-protofilament features, respectively. From now on, these classes will be referred to by their respective protofilament numbers.

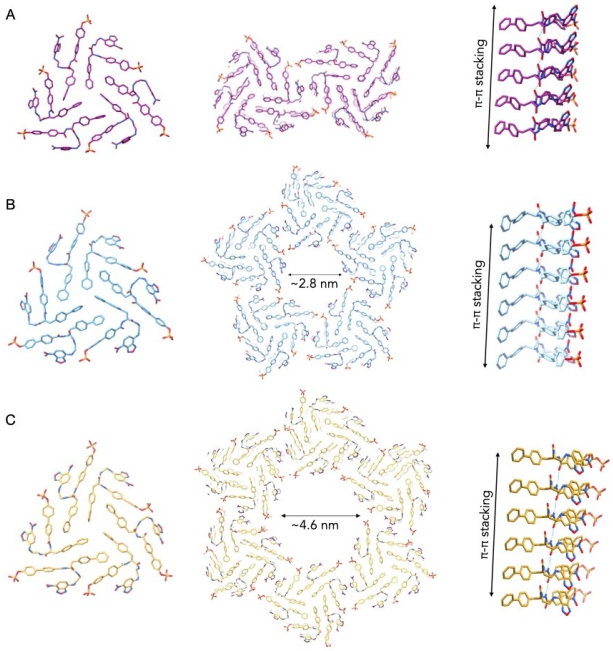

Figure 3. The asymmetric unit (left), the lateral (middle), and the axial interface (right) of three fiber classes are displayed. (A) 2-protofilament fiber; (B) 5-protofilament fiber; (C) 6-protofilament fiber.

The atomic models constructed from 3D reconstructions across three distinct classes reveal a nearly identical asymmetrical unit (ASU), each containing six copies of molecule **1**. These six molecules cluster into a triangle-shaped plate (Figure 3A–C): six hydrophobic biphenyl heads pack centrally, six phosphorylated biphenyl groups project their polar phosphate groups at triangle vertices and midpoints, and NBD rings are positioned between phosphate heads. Within the ASU, the molecule adopts two conformations, with the biphenyl head rotated approximately 180 degrees relative to each other. This suggests the compound may initially form a dimer before assembling into a triangle-shaped plate composed of three such dimers.

When the fiber is sectioned perpendicular to the helical axis and viewed from that axis, 2, 5, and 6 copies of ASUs are clearly visible within the 2-, 5-, and 6-protofilament classes, respectively (Figure 3A–C, Figure S2). Notably, based

on helical symmetries, all protofilaments in these three classes exhibit a slight right-handed twist, with a twist of 1.79°, 1.85°, and 1.32° for 2-, 5-, and 6-protofilament classes, respectively. Within these protofilaments, triangle plates stack atop each other, primarily interacting through pi-stacking contributed by the numerous aromatic rings present in molecule **1** (Figure 3). Hydrogen bonds, reminiscent of canonical β-sheets, are also observed but are not frequent due to the limited number of residues.

While the stacking interface of triangle plates represents the axial interface between ASUs, lateral interactions also exist between ASUs across different protofilaments. Since the triangle plate is nearly perpendicular to the helical axis in all three classes, we can analyze the lateral interactions from the perspective of the helical axis. By connecting three O-atoms (the O-atom linking the P-atom and the biphenyl group) near the triangle vertices, we observe an approximate equilateral triangle when viewed from the axis. Two equilateral triangles (representing two ASUs) interact by sharing half of their side. This interface involves hydrogen bonds between phosphate groups at two edges and interactions between two NBD rings in the middle. Notably, the two triangle sides forming this interface are not perfectly parallel: the rotation angle between these two triangles measures 122.5°, 108.6°, and 122.6°, respectively, for the 2-, 5-, and 6-protofilament classes (Figure 4A–D). This results in a relative angle between the two interacting sides of 2.5°, −11.4°, and 2.6°, respectively, for the 2-, 5-, and 6-protofilament classes. This observation suggests that this favorable interface possesses some plasticity and can accommodate a range of angles.

Based on the cryo–EM structures observed, a plausible self-assembly pathway for molecule 1 can be proposed (Scheme 1). A single molecule **1** consists of three motifs: NBD, BP, and pBP. The initial step is likely the interaction of two BP groups from two separate molecule **1** units, driving dimer formation. Subsequently, three such dimers assemble into a stable building block, the "triangle plate," comprising six copies of molecule **1**. The triangle plates then stack in parallel with a slight right-handed twist, facilitated by extensive pi-stacking interactions between aromatic rings, contributing to the axial growth of the structure. Lateral interactions occur preferentially between specific half sides of two adjacent triangle ASUs, displaying some flexibility with observed rotation angles between 108° and 123°. However, this interface has a limited range of rotation angles it can host. Consequently, only fibers containing 2, 5, or 6 protofilaments are observed. Other configurations, such as 3, 4, or 7 protofilaments, would require a rotation angle between two Figure 4. The interface between two ASUs in three different fiber classes, viewing from the helical axis. (A) 2-protofilament fiber; (B) 5-protofilament fiber; (C) 6-protofilament fiber. The rotation angles between two ASUs are indicated. (D) An overlay of the two ASUs from all three fiber classes highlights the structural variability and adaptability of the interface. ASUs around 60°, 90°, or 129°, respectively, and are notdetected in the self-assembled fiber products.

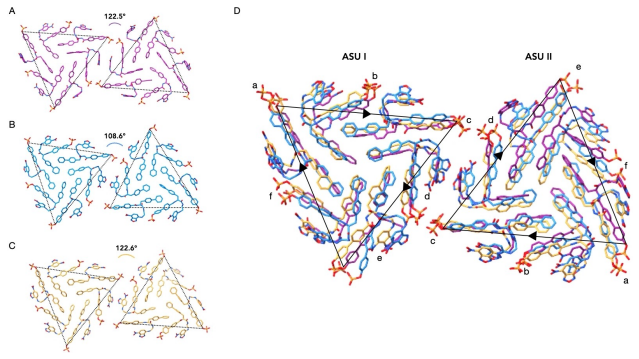

Figure 4. The interface between two ASUs in three different fiber classes, viewing from the helical axis. (A) 2-protofilament fiber; (B) 5-protofilament fiber; (C) 6-protofilament fiber. The rotation angles between two ASUs are indicated. (D) An overlay of the two ASUs from all three fiber classes highlights the structural variability and adaptability of the interface.

When chemically identical subunits interact with each other in ways that are not entirely identical, but involve slight variations, it was originally termed "quasi-equivalence" by Don Caspar and Aaron Klug in their descriptions of icosahedral viruses.[23] We recently reported a similar quasi-equivalence phenomenon in helical tubes showing variable diameters from the cryo–EM study of the spindle-shaped archaeal virus SMV1.[24] We proposed that this might be a common mechanism for helical complexes that rely on diameter changes without significant conformational alterations to achieve their functions, such as BAR domain proteins, ESCRT-III, and dynamin family proteins. How similar are the interactions between ASUs in two helical tubes with differing diameters? Using SMV1 as an example, aligning the protein backbones of two adjacent ASUs from two tubes with substantially different diameters results in a very small RMSD of 0.3–0.4 Å. Interestingly, the RMSD of 624 atoms from two ASUs between 2-, 5-, and 6-start protofilaments is quite large, ranging from 2.6 to 2.9 Å (supplemental Figure 2). Undoubtedly, quasi-equivalence phenomena will also be observed in helical tubes self-assembled from peptide materials. However, based on the observed RMSDs, we believe the structures we reported here differ from quasi-equivalence and should instead be referred to as plasticity.

This phenomenon of interface plasticity – where interfaces are similar enough to be recognized as such, yet display RMSD values significantly larger than those seen in quasi-equivalence – has also been observed in a few other protein and peptide helical polymers. For example, thermophilic archaea *Saccharolobus islandicus* can assemble two distinct type IV pili structures using the same pilin with slightly different helical symmetries (0.3 Å rise and 2° difference per inner core domain). Its N-terminal long helices can accommodate this plasticity in the helical packing.[25] Similarly, PSMα3 peptide nanotubes have been reported to form structures with varying diameters while maintaining a relatively consistent ASU–ASU interface.[26] Furthermore, in the form of peptides, even when peptide lengths are

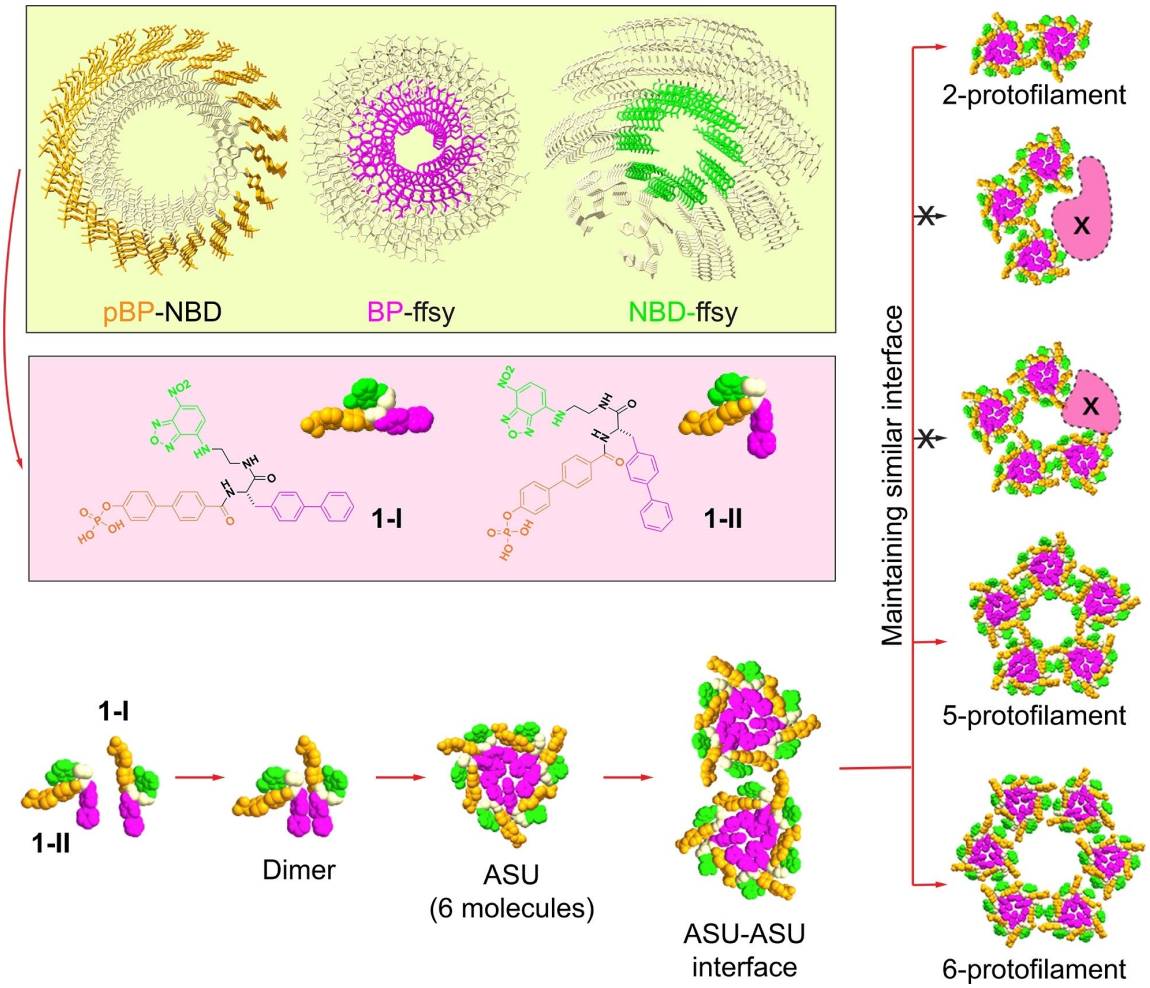

Scheme 1. The fragments (from known nanotubes) generate **1**, two conformations of **1**, and the plausible self-assembly pathway of **1** that forms hierarchical nanotubes.

increased by one or a few heptads, a similar interface is preserved across different peptide designs.[27] Similarly, in this study, we demonstrated that the interface between the triangular ASUs exhibits a moderate degree of plasticity, enabling the formation of multiple nanofiber architectures.

Conclusions

In summary, we determined the near-atomic cryo–EM structures of three nanofibers self-assembled from molecule **1**, which contains distinct fragments from three small molecules that organize into nanotubes. These structures exhibit an almost identical asymmetrical unit (ASU), composed of six molecules, and display a highly similar interface between ASUs in both the axial and lateral directions. Same molecule adopts two conformations to form dimers is common form proteins, but rather scarce for small molecules that self-assemble in water, likely due to limited structure information. For the same reason, this work represents the first case of fragments from known nanotubes, although fragment-based approaches have been implicitly applied in the design of other self-assembling materials, such as liquid crystals. This work underscores the power of cryo–EM in revealing the architecture of self-assembled small molecules, including ultrashort peptides. The observed interaction plasticity provides valuable insights into the principles of small molecule self-assembly and serves as a blueprint for further engineering efforts. Given the existing database of crystal structures for non-peptide small molecules, the growing number of cryo–EM structures of small molecules, and small organic molecules self-assemble in water,[2,28] the pool of molecular fragments available for study will continue to expand. This expansion creates a unique and promising opportunity to apply a fragment-based approach to the design of supramolecular biomaterials. Although the in-situ structure of the assembly of **1** inside cells remain to be established, the potent activity of **1** against immunosupressive cancer cells[15] underscores the promises of this approach. By leveraging these insights, it may be possible to engineer small molecule assemblies

with tailored properties for a variety of applications, including catalysis, drug delivery, and biomaterials science.

Acknowledgements

This research was, in part, supported by the National Cancer Institute's National Cryo–EM Facility at the Frederick National Laboratory for Cancer Research under contract 75N91019D00024. Electron microscopy screening was carried out in the UAB Cryo-EM Facility, supported by the Institutional Research Core Program and O'Neal Comprehensive Cancer Center (NIH grant P30 CA013148), with additional funding from NIH grant S10 OD024978. We are grateful to Dr. James Kizziah and Dr. Adam Wier for assisting with the screening or data collection. The work in F.W. laboratory was supported by NIH grant GM138756. The work in the B. X. laboratory was supported by NIH grants CA142746, CA262920, and EY036512, and the NSF DMR-2011846 MRSEC program at Brandeis.

Conflict of Interests

The authors declare no conflict of interest.

Data Availability Statement

The data that support the findings of this study are openly available in EMDB at https://www.ebi.ac.uk/emdb/, reference number 47087.

Keywords: Hierarchical self-assembly · Fragment-based approach · Plasticity in assembly

[1] a) E. T. Pashuck, H. Cui, S. I. Stupp, *J. Am. Chem. Soc.* **2010**, *132*, 6041–6046; b) Z. Yang, G. Liang, L. Wang, B. Xu, *J. Am. Chem. Soc.* **2006**, *128*, 3038–3043; c) Y. Cai, H. Shen, J. Zhan, M. Lin, L. Dai, C. Ren, Y. Shi, J. Liu, J. Gao, Z. Yang, *J. Am. Chem. Soc.* **2017**, *139*, 2876–2879; d) A. Jain, S. Kassem, R. S. Fisher, B. Wang, T. D. Li, T. Wang, Y. He, S. Elbaum-Garfinkle, R. V. Ulijn, *J. Am. Chem. Soc.* **2022**, *144*, 15002–15007; e) A. Aggeli, I. A. Nyrkova, M. Bell, R. Harding, L. Carrick, T. C. McLeish, A. N. Semenov, N. Boden, *Proc. Natl. Acad. Sci. USA* **2001**, *98*, 11857–11862; f) S. Kiyonaka, K. Sada, I. Yoshimura, S. Shinkai, N. Kato, I. Hamachi, *Nat. Mater.* **2004**, *3*, 58–64; g) C. M. Micklitsch, P. J. Knerr, M. C. Branco, R. Nagarkar, D. J. Pochan, J. P. Schneider, *Angew. Chem. Int. Ed.* **2011**, *50*, 1577–1579; h) M. Samanta, N. Saad, D. Wu, N. S. A. Crone, K. Abramov-Harpaz, C. Regev, R. Cohen-Luria, A. L. Boyle, Y. Miller, A. Kros, G. Ashkenasy, *Angew. Chem. Int. Ed.* **2024**, *64*, e202413810; i) J. Rodon Fores, M. Criado-Gonzalez, A. Chaumont, A. Carvalho, C. Blanck, M. Schmutz, F. Boulmedais, P. Schaaf, L. Jierry, *Angew. Chem. Int. Ed.* **2020**, *59*, 14558–14563; j) C. Jin, G. Li, X. Wu, J. Liu, W. Wu, Y. Chen, T. Sasaki, H. Chao, Y. Zhang, *Angew. Chem. Int. Ed.* **2021**, *60*, 7597–7601; k) A. Dey, E. Naranjo, R. Saha, S. Zhang, M. N. Nair, T. D. Li, X. Chen, R. V. Ulijn, *Angew. Chem. Int. Ed.* **2024**, *63*, e202409391; l) F. Tian, R. C. Guo, C. Wu, X. Liu, Z. Zhang, Y. Wang, H. Wang, G. Li, Z. Yu, *Angew. Chem. Int. Ed.* **2024**, *63*, e202404703; m) H. Yin, Y. Hua, S. Feng, Y. Xu, Y. Ding, S. Liu, D. Chen, F. Du, G. Liang, W. Zhan, Y. Shen, *Adv. Mater.* **2024**, *36*, e2308504.
[2] L. A. Estroff, A. D. Hamilton, *Chem. Rev.* **2004**, *104*, 1201–1218.
[3] X. Du, J. Zhou, J. Shi, B. Xu, *Chem. Rev.* **2015**, *115*, 13165–13307.
[4] a) P. Majumder, U. Baxa, S. T. R. Walsh, J. P. Schneider, *Angew. Chem. Int. Ed.* **2018**, *57*, 15040–15044; b) W. Zhan, L. Xu, Z. Liu, X. Liu, G. Gao, T. Xia, X. Cheng, X. Sun, F. G. Wu, Q. Yu, G. Liang, *Angew. Chem. Int. Ed.* **2023**, *62*; c) G. Liang, J. Ronald, Y. Chen, D. Ye, P. Pandit, M. L. Ma, B. Rutt, J. Rao, *Angew. Chem. Int. Ed.* **2011**, *50*, 6283–6286; d) R. An, X. Cheng, S. Wei, Y. Hu, Y. Sun, Z. Huang, H. Y. Chen, D. Ye, *Angew. Chem. Int. Ed.* **2020**, *59*, 20636–20644.
[5] C. H. Gorbitz, *Chemistry* **2001**, *7*, 5153–5159.
[6] M. Reches, E. Gazit, *Science* **2003**, *300*, 625–627.
[7] a) T. M. Clover, C. L. O'Neill, R. Appavu, G. Lokhande, A. K. Gaharwar, A. E. Posey, M. A. White, J. S. Rudra, *J. Am. Chem. Soc.* **2020**, *142*, 19809–19813; b) S. Liu, Q. Zhang, A. N. Shy, M. Yi, H. He, S. Lu, B. Xu, *J. Am. Chem. Soc.* **2021**, *143*, 15852–15862.
[8] a) J. Shi, X. Du, D. Yuan, J. Zhou, N. Zhou, Y. Huang, B. Xu, *Biomacromolecules* **2014**, *15*, 3559–3568; b) C. H. W. A. Corbet, B. W. L. van den Bersselaar, B. F. M. de Waal, R. Reynaerts, K. S. Mali, S. De Feyter, A. M. Jonas, E. W. Meijer, G. Vantomme, *Chem. Eur. J.* **2024**, *30*, e202303107.
[9] Z. Yang, G. Liang, M. Ma, Y. Gao, B. Xu, *J. Mater. Chem.* **2007**, *17*, 850–854.
[10] F. Sheehan, D. Sementa, A. Jain, M. Kumar, M. Tayarani-Najjaran, D. Kroiss, R. V. Ulijn, *Chem. Rev.* **2021**, *121*, 13869–13914.
[11] E. H. Egelman, C. Xu, F. Dimaio, E. Magnotti, C. Modlin, X. Yu, E. Wright, D. Baker, V. P. Conticello, *Structure* **2015**, *23*, 280–289.
[12] a) Z. Feng, H. Wang, F. Wang, Y. Oh, C. Berciu, Q. Cui, E. H. Egelman, B. Xu, *Cell Rep Phys Sci* **2020**, *1*, 100085; b) J. Guo, F. Wang, Y. Huang, H. He, W. Tan, M. Yi, E. H. Egelman, B. Xu, *Nat. Nanotechnol.* **2023**, *18*, 1094–1104; c) R. R. Sonani, S. Bianco, B. Dietrich, J. Doutch, E. R. Draper, D. J. Adams, E. H. Egelman, *Cell Rep Phys Sci* **2024**, *5*, 101812; d) A. Bigo-Simon, L. F. Estrozi, A. Chaumont, R. Schurhammer, G. Schoehn, J. Combet, M. Schmutz, P. Schaaf, L. Jierry, *ACS Nano* **2024**, *18*, 30448–30462.
[13] a) D. A. Erlanson, S. W. Fesik, R. E. Hubbard, W. Jahnke, H. Jhoti, *Nat. Rev. Drug Discovery* **2016**, *15*, 605–619; b) K. Babaoglu, B. K. Shoichet, *Nat. Chem. Biol.* **2006**, *2*, 720–723.
[14] a) J. E. Padilla, C. Colovos, T. O. Yeates, *Proc. Natl. Acad. Sci. USA* **2001**, *98*, 2217–2221; b) N. P. King, W. Sheffler, M. R. Sawaya, B. S. Vollmar, J. P. Sumida, I. André, T. Gonen, T. O. Yeates, D. Baker, *Science* **2012**, *336*, 1171–1174.
[15] M. Yi, G. Ashton-Rickardt, W. Tan, Z. Liu, H. He, J. T. Hsieh, B. Xu, *Chemistry* **2024**, *30*, e202400691.
[16] M. Yi, F. Wang, W. Tan, J. T. Hsieh, E. H. Egelman, B. Xu, *J. Am. Chem. Soc.* **2022**, *144*, 13055–13059.
[17] A. Deshmukh, W. Zheng, C. Chuang, A. Bailey, J. Williams, E. Sletten, E. Egelman, J. Caram, *Nat. Chem.* **2024**, *16*, 800–808.
[18] J. Guo, S. T. Rich-New, C. Liu, Y. Huang, W. Tan, H. He, M. Yi, X. Zhang, E. H. Egelman, F. Wang, B. Xu, *Chem* **2023**, *9*, 2530–2546.
[19] F. Wang, O. Gnewou, A. Solemanifar, V. P. Conticello, E. H. Egelman, *Chem. Rev.* **2022**, *122*, 14055–14065.
[20] Y. Yang, D. Arseni, W. Zhang, M. Huang, S. Lovestam, M. Schweighauser, A. Kotecha, A. G. Murzin, S. Y. Peak-Chew, J. Macdonald, I. Lavenir, H. J. Garringer, E. Gelpi, K. L. Newell, G. G. Kovacs, R. Vidal, B. Ghetti, B. Ryskeldi-Falcon, S. H. W. Scheres, M. Goedert, *Science* **2022**, *375*, 167–172.
[21] A. W. P. Fitzpatrick, B. Falcon, S. He, A. G. Murzin, G. Murshudov, H. J. Garringer, R. A. Crowther, B. Ghetti, M. Goedert, S. H. W. Scheres, *Nature* **2017**, *547*, 185–190.
[22] Y. Yang, Y. Shi, M. Schweighauser, X. Zhang, A. Kotecha, A. G. Murzin, H. J. Garringer, P. W. Cullinane, Y. Saito, T. Foroud, T. T. Warner, K. Hasegawa, R. Vidal, S. Murayama, T. Revesz, B. Ghetti, M. Hasegawa, T. Lashley, S. H. W. Scheres, M. Goedert, *Nature* **2022**, *610*, 791–795.
[23] D. L. Caspar, A. Klug, *Cold Spring Harb Symp Quant Biol* **1962**, *27*, 1–24.
[24] F. Wang, V. Cvirkaite-Krupovic, M. Vos, L. C. Beltran, M. A. B. Kreutzberger, J. M. Winter, Z. Su, J. Liu, S. Schouten, M. Krupovic, E. H. Egelman, *Cell* **2022**, *185*, 1297–1307 e1211.
[25] J. Liu, G. N. Eastep, V. Cvirkaite-Krupovic, S. T. Rich-New, M. A. B. Kreutzberger, E. H. Egelman, M. Krupovic, F. Wang, *Nat. Commun.* **2024**, *in press*.
[26] M. A. B. Kreutzberger, S. Y. Wang, L. C. Beltran, A. Tuachi, X. B. Zuo, E. H. Egelman, V. P. Conticello, *P Natl Acad Sci USA* **2022**, *119*, e2121586119.
[27] F. Wang, O. Gnewou, C. Modlin, L. C. Beltran, C. Xu, Z. Su, P. Juneja, G. Grigoryan, E. H. Egelman, V. P. Conticello, *Nat. Commun.* **2021**, *12*, 407.
[28] a) A. Angelova, M. Drechsler, V. M. Garamus, B. Angelov, *ChemNanoMat* **2019**, *5*, 1381–1389; b) D. Liu, A. Angelova, J. Liu, V. M. Garamus, B.

Angelov, X. Zhang, Y. Li, G. Feger, N. Li, A. Zou, *J. Mater. Chem. B* **2019**, *7*, 4706–4716.

[29] a) S. Q. Zheng, E. Palovcak, J.-P. Armache, K. A. Verba, Y. Cheng, D. A. Agard, *Nat. Methods* **2017**, *14*, 331–332; b) A. Rohou, N. Grigorieff, *J. Struct. Biol.* **2015**, *192*, 216–221; c) F. Wang, O. Gnewou, A. Solemanifar, V. P. Conticello, E. H. Egelman, *Chem. Rev.* **2022**, *122*, 14055–14065; d) R. Sanchez-Garcia, J. Gomez-Blanco, A. Cuervo, J. M. Carazo, C. O. S. Sorzano, J. Vargas, *Communications Biology* **2021**, *4*, 874; e) N. W. Moriarty, R. W. Grosse-Kunstleve, P. D. Adams, *Acta Crystallographica Section D* **2009**, *65*, 1074–1080; f) P. Emsley, K. Cowtan, *Acta Crystallographica Section D* **2004**, *60*, 2126–2132; g) P. V. Afonine, B. K. Poon, R. J. Read, O. V. Sobolev, T. C. Terwilliger, A. Urzhumtsev, P. D. Adams, *Acta Crystallographica Section D* **2018**, *74*, 531–544.

Manuscript received: December 16, 2024
Accepted manuscript online: February 13, 2025
Version of record online: February 25, 2025